fluids

MDPI

Article

Piezo-Plunger Jetting Technology: An Experimental Study on Jetting Characteristics of Filled Epoxy Polymers

Alexander Kurz [1,2,*], Jörg Bauer [1] and Manfred Wagner [2]

[1] Fraunhofer Institute for Reliability and Microintegration (IZM), System Integration and Interconnection Technologies, Gustav-Meyer-Allee 25, D-13355 Berlin, Germany; Joerg.Bauer@izm.fraunhofer.de

[2] Berlin Institute of Technology (TU Berlin), Polymer Engineering and Physics, Ernst-Reuter-Platz 1, D-10587 Berlin, Germany; manfred.wagner@tu-berlin.de

* Correspondence: dr.alexander.kurz@gmx.de; Tel.: +49-30-314-24758; Fax: +49-30-314-21108

Received: 4 December 2018; Accepted: 22 January 2019; Published: 1 February 2019

Abstract: The droplet formation of Newtonian fluids and suspensions modified by spherical, non-colloidal particles has attracted much interest in practical and theoretical research. For the present study, a jetting technique was used which accelerates a geometrically defined plunger by a piezoelectric actuator. Changing rheological properties of materials and extending deformation rates towards nonlinear viscoelastic regimes created the requirement to extend dosage impulses towards larger magnitudes. To mimic the rheological characteristics of nonconductive adhesives we modified Newtonian epoxy resins by thixotropic additives and micro-scale glass spheres. Rheological analysis at steady shear and oscillatory shear ensured a differentiation between material and process-related factors. Evaluation of high-speed images allowed the investigation of drop dynamics and highlighted the dispense impulse reduction by material-specific dampening properties.

Keywords: complex fluids; drop formation; epoxy; jetting; polymers; polymer processing; prototyping; rheology

1. Introduction

The progressive evolution of micro-systems technology and its transition into consumer products requires continuous miniaturization of electronic components. The first step in the development of chip interconnection technology for advanced applications is the combination of electronic and optoelectronic devices for which suitable support structures are essential. For this strategic aim, jetting with piezo-controlled dosing valves is a technology with high potential due to its adaptability and flexibility. By only a few changes in dosing mechanics, this widely used technology can be customized from inkjet applications towards new and more complex materials [1,2]. General requirements for dispensing small quantities of fluids by jetting are high spatial resolution and short process times. To fulfill these requirements, it is necessary to improve the understanding of drop formation pinch-off and thread movement for fluids with complex rheological behavior [3]. As discussed in the following, fundamental differences exist in comparison to recent studies (as detailed below) on fluid application, drop formation, or dot deformation for plunger-based dispensing methods of paste-like fluids at short dosage times.

2. Background

Drop formation and drop constriction are intensively investigated topics of research. The wide interest in analyzing these phenomena in the context of jetting has resulted in an increasing number

of scientific discourses. Major topics are, for example, studies on complex materials [4–7], on drop formation stages [8–11], or changes of the dispense mechanisms applied [11–15].

Dong, Carr, and Morris [16] focused their experimental research on drop-on-demand (DOD) formation. In combination with a piezoelectric inkjet print head and a 53-µm nozzle orifice, the authors used water and water-glycerin mixtures. A shockwave was directly coupled into the fluid leading to five stages of drop formation. Pinch-off from the nozzle orifice occurred during the stretching phase (primary break-up) whereas end-pinching evolved during the contraction phase (secondary break-up). With increasing surface tension and/or decreasing viscosity, the dispensed volumes of the primary drop and satellite drops increased. Additionally, the break-up depended critically on the fluid properties as well as on the type of shockwave applied.

Investigations by Rother, Richter, and Rehberg [17] focused on the pinch-off itself and revealed three categories of fluid flow. Drop formation measurements were executed by use of water-glycerin mixtures while the droplet release was induced only by gravitational and capillary forces. During the initial stage, drop shrinkage was observed in close proximity to the pinch point with the initiation of a self-similar motion. Two separate flow regimes became discernible by the transition from a viscosity-dominated Stokes regime towards an inertia-dominated Navier–Stokes regime which led to a slope change in the shrinkage velocity of the neck diameter. The transition points depended on the fluid viscosity. Due to self-similar motion, the classical linear stability analysis failed.

Henderson, Pritchard, and Smolka [18] analyzed the pinch-off of low-viscosity Newtonian fluids in a pendant drop setup with gravitationally induced drop detachment. Detailed observations of the fine structure of secondary breakups revealed wavelike instabilities which led to multiple breakups and a comprehensive number of satellite droplets. The primary pinch-off started with a monotonous necking near the drop and led to simultaneous breakups at different thread locations. Wavelike instabilities were not observed for the primary thread but were generated during the breakup stage.

Computational models give additional insight into drop formation characteristics. Xu and Basaran [19] focused their work on the detachment of incompressible Newtonian fluids from a 10-µm capillary. They used Galerkin/finite element method (FEM) methods to characterize the stripping of monodisperse droplets from a DOD-inkjet valve. The first of two stages started with an increasing fluid volume ejection directed to the nozzle orifice. Subsequently, a constant flow rate could be calculated. With increasing process time, the piezo actuator relaxed and the second phase commenced with reflux of the fluid. This stage was referred to as the meniscus retraction stage. Fluid inertia and disturbances led to drop shrinkage and primary drop breakup. For the starting time of flow inversion during jetting, the authors found a correlation with the Ohnesorge number. Additionally, the Weber number was used to characterize a positive axial velocity of the lower drop fragment and the meniscus retraction to the capillary orifice. Reflecting the importance of the Ohnesorge and Weber numbers, the authors developed a phase diagram for DOD drop formation.

The scope of the present research was to achieve a better understanding of mechanisms in plunger-based DOD drop formation for highly filled polymers. In contrast to studies on inkjet printing of Newtonian fluids or diluted polymer solutions [20,21] with equilibrium droplet constriction or pendant drop setups [17,22], a massive jet impulse is required for highly filled fluids. As a compromise between minimization of the drop size and microscale particle-based polymer modifications, we choose a nozzle orifice of 100 µm. The modifications of fluids investigated started with neat Newtonian resins and successively included high concentrations of thixotropic nanoscale additives and microscale glass spheres. The jetting process used is characterized by high-speed fluid deformation and short dispensing times. We could distinguish between dominating process conditions and optimal rheological properties for commercial adaption of the jetting process, e.g., in chip interconnection technologies.

3. Experimental

3.1. Materials

The selection of materials and their modification was motivated by the relevant application properties, see Table 1. Starting with Newtonian flow characteristics of different epoxy resins we increased the rheological complexity of the fluids by the addition of nanoscale and microscale inorganic fillers.

Table 1. Material composition overview.

Material Category	Matrix Resin	Microscale Filler (Glass Spheres)		Nanoscale Filler (Aerosil R805)	Fluid Characteristic	Sample Name
		wt.-%	Diameter	wt.-%		
I.	REPDTP	-	-	-	Newtonian	REPDTP
	REPDTP	-	-	5	Thixotropic	REPDTP-R
	R0161	-	-	-	Newtonian	R0161
	R0161	-	-	5	Thixotropic	R0161-R
II.	R0161	62	<24 µm	-	Newtonian-like	R0161-SiO
	R3001	Commercial system	<24 µm	-	Newtonian-like	R3001
III.	REPDTP	62	<24 µm	2	Paste-like	REPDTP-R-SiO
	R0161	62	<24 µm	2	Paste-like	R0161-R-SiO

To investigate the influence of nanoscale fillers on fluid cohesion by increasing elasticity and thixotropy, the Newtonian resins REPDTP[1] and R0161[2] (material category I) were modified by adding 5 wt.-% Aerosil R805[3]. The fluids of category II are equivalent to so-called Underfillers which are widely used in microsystems technology. They show Newtonian-like flow behavior but also include glass spheres[4] with diameters of around 20 µm (microscale fillers) at a typical concentration of 60–70 wt.-%. To avoid any kind of sedimentation only the high viscosity resin, R0161 was used as a matrix for the category II fluids which were compared with the commercial Underfiller R3001[5]. With fluids of category III of the material matrix, we aimed to investigate both epoxy resins REPDTP[6] and R0161[7] with the added combination of the nanoscale thixotropic agent Aerosil R805 and microscale glass spheres. To ensure a comparison between category II and category III fluids, we kept the glass sphere concentration at 62 wt.-%, but reduced the Aerosil R805 concentration to 2 wt.-% to guarantee optimal dispersion of the fillers.

1 Ruetapox EPD TP (Trimethylolpropane triglycidyl ether, Martin Aerospace, Los Angeles, CA, USA)
2 Ruetapox 0161 (Bisphenol F Diglycidyl ether)
3 AEROSIL R805 (Business Line AEROSIL®, Evonik Degussa GmbH, Essen, Germany)
4 SPHERIGLASS®Solid Glass Spheres: A Glass, Product Grade 5000 (Potters Industries Inc., Malvern, PA, USA)
5 R3001iEX Nagase ChemteX Corporation (Osaka, Japan)
6 Ruetapox EPD TP (Trimethylolpropane triglycidyl ether)
7 Ruetapox 0161 (Bisphenol F Diglycidyl ether)

3.2. Jetting Apparatus

Considering the complex rheology of the test fluids, a plunger-based jetting technique had to be selected. The piezoelectric actuator ensured a well-defined material dosage. Small dimensional changes of the actuator are induced by electrical impulses and are translated into high plunger paths (needle lifts) with the assistance of a lever arm. As soon as the jetting sequence is triggered, the plunger moves upwards to a defined position that is given as a percentage of the overall plunger path. The jetting valve opens, and the test liquid is delivered into the fluidic module. To achieve high dosage impulses

and ensure jetting of all viscous and paste-like fluids at the same comparable parameter set, the needle lift is set to its maximum height of 100%. Subsequently, the plunger is accelerated downwards to the nozzle (falling step). Due to the motion characteristic of the plunger, its kinetic energy is transferred to the test liquid and pushes the material through the nozzle orifice. Figure 1 shows a schematic of the needle lift as a function of time for a typical dispense sequence.

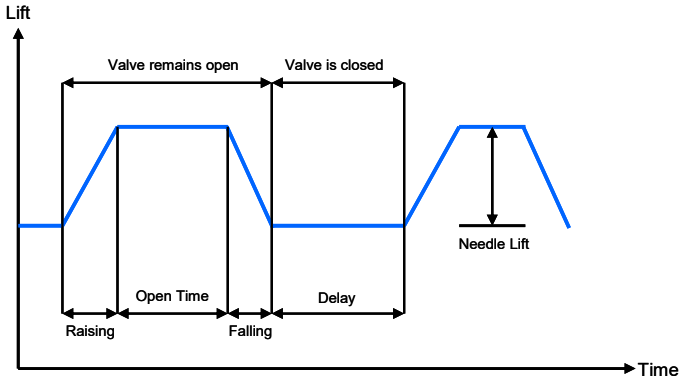

Figure 1. Schematic of dispense sequence and relevant process parameters.

The influence of individual motion parameters on the jetting process is obvious and, in combination with various nozzles and plunger geometries, a significant diversity of trigger impulses is achievable. Considering different materials with different relaxation times, zero-shear viscosities, and fluctuating networks, diverse dispense characteristics can be expected. When jetting particle-filled fluids, it is also important to avoid particle squeezing. Therefore, it is essential to use nozzles with a diameter of at least four to five times larger than the particle diameter. Thus, we choose a nozzle diameter of 100 µm for all experiments to avoid particle squeezing and nozzle blockage and, at the same time, to achieve the minimal drop diameters possible since the nozzle orifice and drop diameter are proportional to each other.

We used a ceramic plunger with a diameter of 1.5 mm for all of the fluid compositions examined, since it is superior with regard to the reduction of particle aggregation in comparison to metal plungers, and it provides the best fit to the inner nozzle curvature. By implementation of the high-speed camera Motion Pro-HS4 (Redlake MASD, LLC, Tucson, AZ, USA) and a zoom lens, drop formation and drop deformation at high dosage velocities were recorded. The magnification remained fixed and drop images were collected in a "free fall position" without a view of the target substrate (see Figure 2 for the camera placement). To achieve stable droplet geometries, the dispensing was performed in a so-called burst mode which is defined as jetting an infinite series of droplets at a set of fixed parameters. A delay time of 400 ms was programmed between drops while the image recording was triggered at every tenth drop.

With respect to high magnification and fast image sequences of 35,000 frames per second, a cold light source was used ensuring high light intensities without heating the test liquids. The test temperature was stabilized at 25 °C.

An ARES G2 rheometer (TA Instruments, New Castle, DE, USA) with plates of 25 mm in diameter in a plate-plate geometry and a gap of 500 µm was used to collect shear flow data. To correlate the rheological measurements with jetting experiments a test temperature of 25 °C was also used for the shear experiments. In order to investigate and correlate the complex rheology of the samples with a drop-on-demand formation, a wide range of shear flow conditions was applied. Shear rate sweeps were performed in the range of 0.001 s^{-1} to 1000 s^{-1}, as well as strain sweeps with oscillatory shear at 6 rad/s from 0.001% to 100% shear deformation.

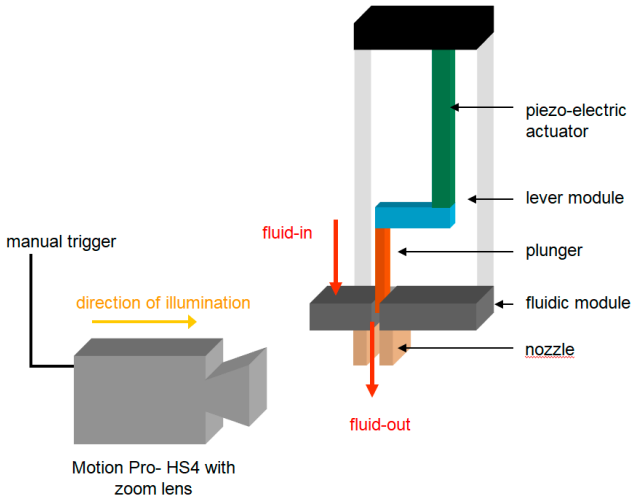

Figure 2. Experimental setup of jetting apparatus and high-speed image acquisition.

3.3. Material Deformation during Plunger-Based Jetting

Substantial dosage impulses had to be applied to utilize the valve system for dispensing high-viscosity materials with increasing shear rates in the nozzle orifice. In order to achieve a suitable correlation between the jetting sequence and fluid properties, laser vibrometer measurements of the path of the plunger (needle lift) were performed. In Figure 3 a plot of two dispense phases as a function of time is presented.

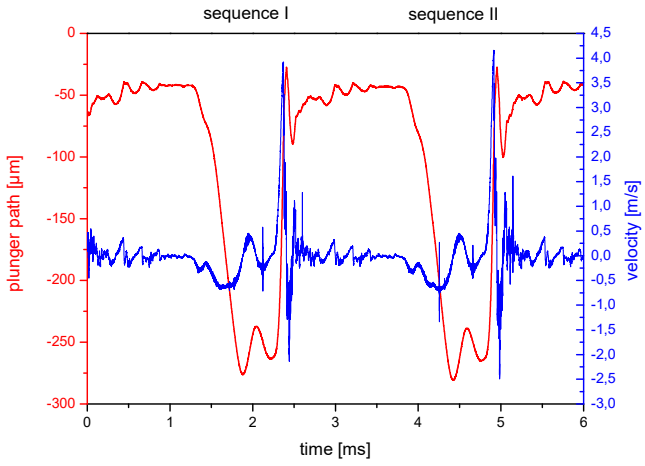

Figure 3. Laser vibrometer measurement of the linear plunger path as a function of time; parameters: Rt 0.5 ms, Ft 0.1 ms, Ot 0.5 ms, 100% needle lift.

For the jetting parameters indicated in Figure 3 a plunger velocity of 4.16 m/s and a needle lift of 234 µm were measured. The equation of Hagen and Poiseuille was used to calculate the maximum shear rate during the first jetting phase. Hereby, fluid incompressibility and a non-damped impulse transfer from the plunger to the dispensed fluid are valid assumptions. For a single-sided open valve geometry, a maximum shear rate of 3.8×10^4 s^{-1} was found, which led to solid-like fluid deformation.

4. Results

4.1. Rheological Characterization of Test Fluids

The change in shear flow behavior of the neat and modified epoxy resins is documented by shear rate sweeps, as shown in Figures 4 and 5. Newtonian flow behavior for the unmodified fluids is verified

at the shear rate range investigated with viscosities of 150 mPa·s for REPDTP and 3700 mPa·s for R0161. For thixotropic modifications with Aerosil R805, a distinct correlation between shear rate and viscosity is observed. Due to the strong polarization effects of the Aerosil R805 nanoparticles, a temporary network of secondary forces is created in the polymer leading to a viscosity increase by several orders of magnitude. Increasing shear rates weaken the secondary forces and shear thinning results from a breakdown of the superstructure. By plotting shear stress as a function of shear rate, it can be observed that REPDTP-R is a plastic fluid with a yield stress and R0161-R is a pseudo-plastic fluid.

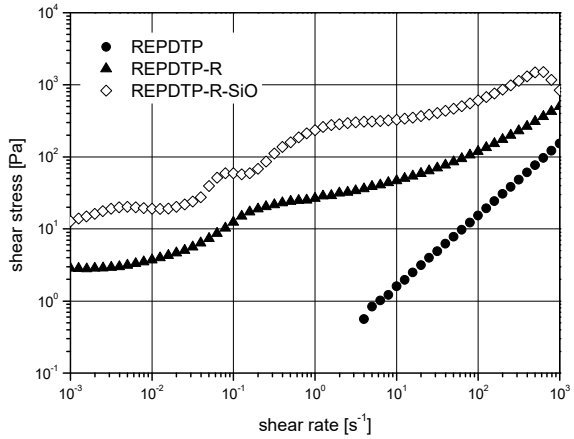

Figure 4. Shear rate sweeps of REPDTP and its modifications.

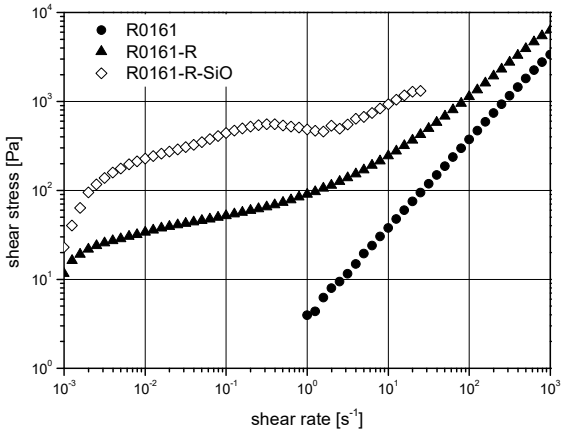

Figure 5. Shear rate sweeps of R0161 and its modifications.

The rheological data for REPDTP-R as a function of shear rate feature deviations from a monotonous trend. In contrast to other standard epoxy resins, a dilatancy plateau appears at a shear rate of 0.1 s^{-1}. Given the fact that Aerosil R805 is characterized by high nanoparticle polarity and additionally, by A high surface-to-volume ratio, the dipole interactions between the epoxy resin and polar additive lead to temporary network formation. The epoxy system REPDTP is a technical grade which is not fully epoxidized, and small quantities of polar groups remain in the resin. This leads to further network stabilization by long-range interactions of polar polymer groups with Aerosil R805. Up to shear rates of 0.1 s^{-1}, a moderate network deformation translates into nanoparticle orientation parallel to the flow direction. The viscosity decreases, and a viscosity plateau is reached at a shear rate of approximately 0.1 s^{-1}. However, due to its inherent nature, the superstructure is relatively weak and becomes gradually destroyed with increasing shear rates. The flow resistance is weakened in favor of a statistical distribution of the nanoparticles.

A combination of the resins REPDTP or R0161 with nanoscale fillers and glass spheres increases the shear viscosity substantially (materials of category III, Figures 4 and 5). The so-called dispersions

show a pseudo-plastic characteristic. In comparison with REPDTP-R and R0161-R, the viscosity increases by one order of magnitude due to the addition of glass spheres. Furthermore, particle–particle interactions affect the low-shear regime around 0.002 s^{-1} for R0161-R-SiO and the superstructure plateau of REPDTP-R-SiO around 0.1 s^{-1} by an increase of flow resistance.

Figure 6 presents a shear rate sweep of fluids of material category II. As mentioned earlier, Underfillers consist of a low-viscosity polymer matrix and glass fillers of several micrometers in diameter. Incorporating a thixotropic effect in the property catalog of these materials is essential for achieving an optimized flow at low shear rates driven only by capillary forces. For system R0161-SiO, the steric impediment which is caused by particle–particle interactions can clearly be observed in the low-shear regime. Due to the lack of network formation, hard elastic effects dominate the flow behavior. Above 0.01 s^{-1}, a viscosity plateau is observed over a significant shear rate range. The second viscosity drop at high shear rates is caused by a breakdown of internal cohesion. Due to sensitivity limitations of the rheometer, the used shear rate sweeps of low-viscosity materials such as R 3001 are only reliable at shear stresses above 1 Pa. The observation of a constant shear stress slope for the test system is in accordance with the behavior of commercial Underfiller R 3001.

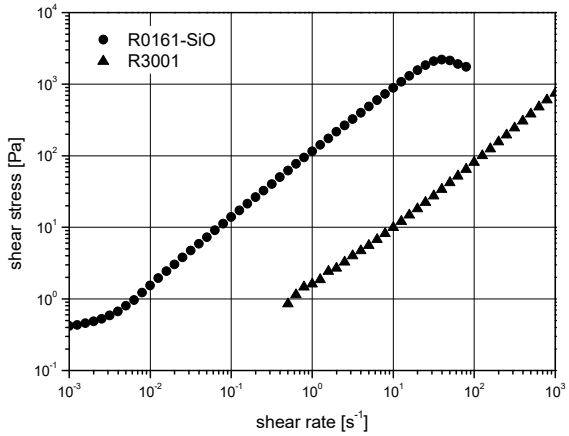

Figure 6. Shear rate sweeps of category II Underfillers.

To determine sol and gel states, as well as the sol-gel transition strain, sweep tests under oscillatory shear at a frequency of 6 rad/s were performed and are presented in Figure 7. Due to limited stress responses of low-viscosity fluids at small shear deformations, a critical value of the shear strain has to be reached in order to measure the storage modulus, G′, and loss modulus, G″, accurately. tan δ is referred to as the loss factor and is obtained as a ratio of the loss modulus G″ to storage modulus G′. It is important to note that a loss factor tan $\delta > 1$ describes a gel state while a loss factor $\delta < 1$ indicates a sol state of the viscoelastic fluid. According to the Winter–Chambon Spectrum [23], the so-called gel point is reached at a frequency-independent loss factor close to tan $\delta = 1$. For the Newtonian systems REPDTP and R0161, a sol state at a constant modulus can be verified for the deformation range investigated. One can easily identify the viscosity difference between the two fluids by the different values of the loss moduli G″, see Figure 7A,B.

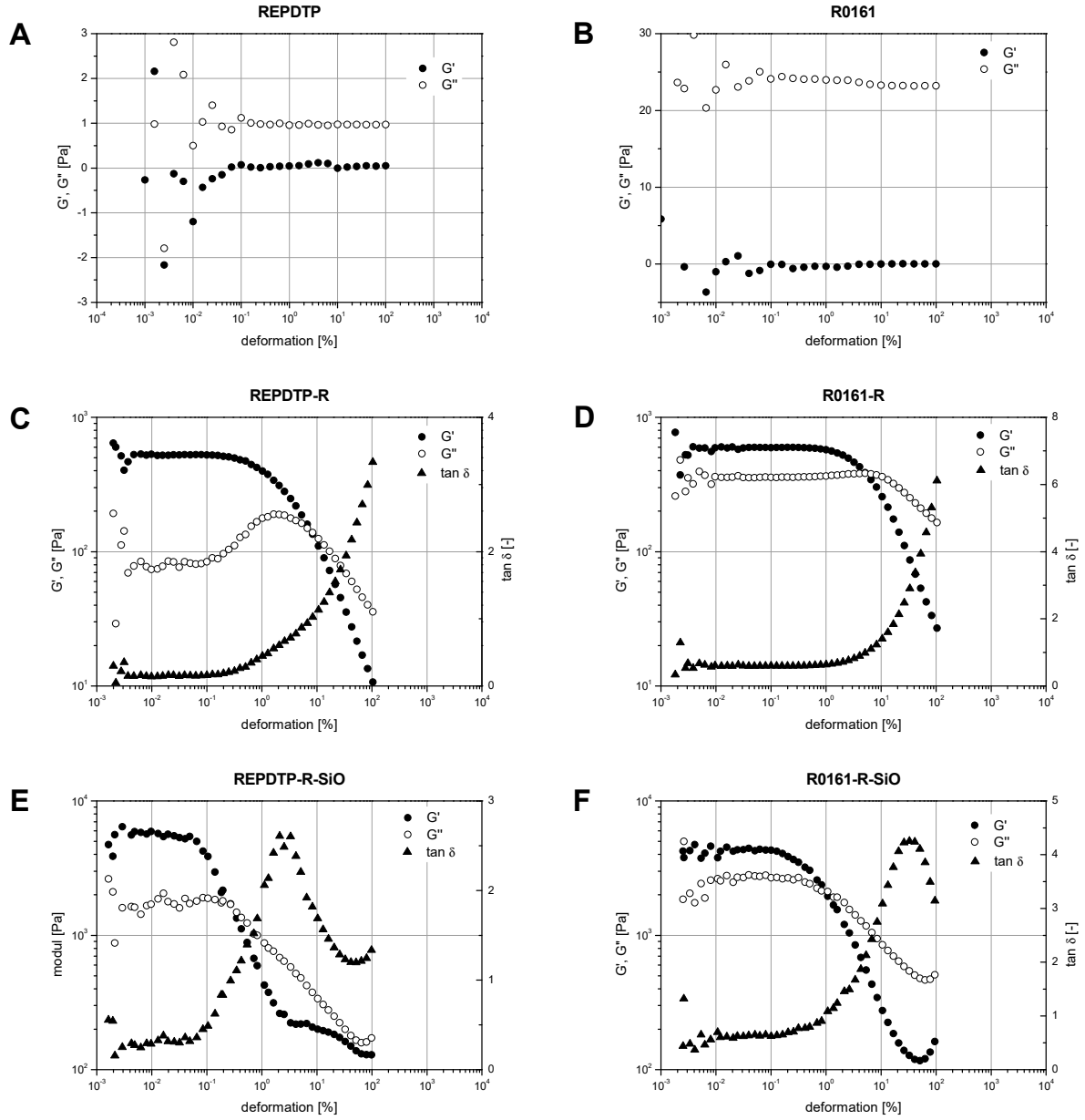

Figure 7. Strain sweep tests under oscillatory shear at 6 rad/s; material category I (**A**–**D**) and material category III (**E**,**F**).

The thixotropic modification, see Figure 7C,D, leads to a significant change in the material response. At low values of deformation, both materials show a linear viscoelastic response, i.e., G′ and G″ remain constant and independent of the shear deformation. Since the values of G′ are larger than the values of G′, the materials are in the gel state under these conditions. When the non-linear viscoelastic regime is reached, a transition of the materials towards a sol state is observed. For both systems, the storage modulus G′ decreases and the loss modulus G″ increases with increasing shear deformation. The characteristic slope of G″ is more pronounced for REPDTP-R compared to R0161-R and can be related to the superstructure effect discussed earlier. The resistance against structural deformations results from dipole interactions between polar groups of the resin and of the thixotropic additive which leads to an energy dissipation threshold for network deformation and network destruction. Given the fact that the resin R0161 is of higher purity than the technical grade REPDTP, the effects and consequences of the superstructure are negligible for R0161. Nevertheless, the storage moduli G′ are comparable for REPDTP-R and R0161-R since the same quantities of Aerosil R805 are used and

dynamic networks with equivalent levels of stability are formed. Differences in the underlying resin chemistry translate into individual G″ values and correspond with specific viscosities.

Both test systems of category III show an equivalent flow behavior in comparison with modified materials of category I, but with a Newtonian transition at smaller shear strain values, see Figure 7E,F. A key factor is the enhanced local shear strain in the vicinity of the glass spheres. Similar to the thixotropic modifications REPDTP-R and R0161-R, storage moduli of REPDTP-R-SiO and R0161-R-SiO are also comparable whereas the dissipative effect of glass spheres leads to a higher G″ level. For increasing shear strains, a peak in the loss tangent is found which is caused by hard elastic particle interactions between the glass spheres.

As discussed earlier, Underfillers show a viscosity plateau over a wide shear rate range. Due to a Newtonian flow, characteristic sol states are observed in strain sweeps for R0161-SiO and R3001 with a nearly constant loss modulus G″, see Figure 8. Although elastic softening is negligible for R0161-SiO, a local minimum in the storage modulus G′ is seen with increasing deformation indicating the presence of hard elastic interactions of glass spheres. In agreement with viscosity measurements accomplished by strain rate sweeps, the loss modulus G″ of Underfiller R3001 is lower by several orders of magnitude compared to the model system R0161-SiO.

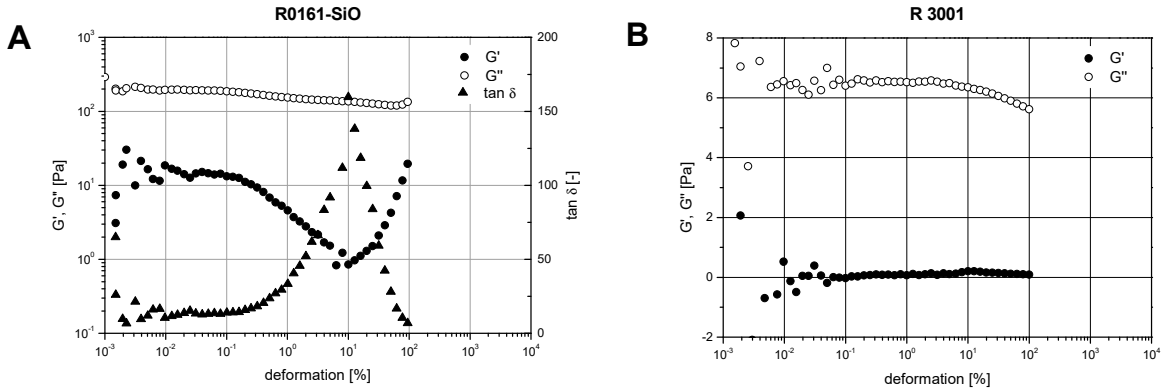

Figure 8. Strain sweep tests under oscillatory shear at 6 rad/s of material category II.

4.2. Plunger-Initiated Drop Formation

Figure 9 shows a schematic of the two jet stages as they evolve with time. For further analysis, we define a reference time, t_0, which corresponds to the time when the material exits the orifice. Jet phase I (from t_0 to t_1) is characterized by (a) moderate flow rates out of the nozzle, (b) by the plunger being in a raised position, and (c) an open valve status. Because of slow fluid accumulation at the nozzle orifice, a standard drop with spherical shape is formed. As soon as the opening interval reaches its pre-defined end-stage, the plunger is accelerated continuously downwards up to its maximum velocity. A major amount of fluid is subsequently pushed through the nozzle and the primary drop undergoes a geometrical change from a spherical to a primary thread (interval t_1 to t_2). When the plunger makes contact with the nozzle pan, vibrational states are injected into the primary thread and stage II of the jet process is reached. The primary thread elongates successively as the plunger impulse moves through the fluid and accelerates the tip.

To analyze the drop evolution, we defined two position parameters (x_1 and x_2) and followed their evolution in time. x_1 marks the beginning of the primary drop whereas x_2 refers to the primary drop end. Depending on the rheological characteristics of the fluid, the primary drop can transition into a primary thread. Hereby, the thread tip and thread end propagate at different velocities leading to primary thread elongation and thus to different slopes of the x_1 and x_2 curves as a function of time.

All geometrical changes are linked to the reference (trigger) time and the progressive time frame counting of the high-speed recording. Due to the field of view limitations, not all parameters are

observable within one high-speed image until the thread breakup. Therefore, drop deformations which occur at the target substrate are not discussed in this study.

In contrast to other studies related to drop formation and drop deformation, we do not consider surface tension effects between the nozzle and fluid. Even for long dispense intervals, surface tension is insignificant compared to the dominance of the plunger impulse and thread contraction was not observed even for Newtonian systems.

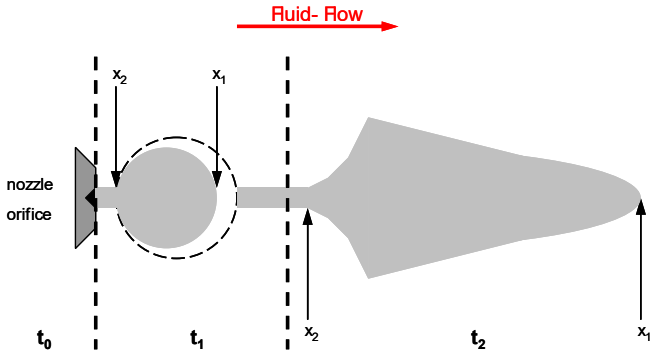

Figure 9. Schematic dispense progress over time.

4.2.1. Category I, Newtonian, and Thixotropic Materials

In this study, REPDTP is the system with the lowest structural stability and viscosity. Both phases of jet deformation are accessible and allow documentation of the drop development. Images 1 to 4 of Figure 10 show slow fluid accumulation at the nozzle orifice in phase I. The fluid exits the orifice at a low velocity until the opening time ends and the plunger acceleration starts. As soon as the plunger hits the nozzle pan, the impulse carries over to the epoxy resin (frame 5) and stretches the primary drop to a primary thread. The thread tip continues elongating while the filament end and the liquid tail move with lower velocity (images 6 to 9). The stretching of the filament leads to a reduction in the diameter and to multiple wavelike breakups (frame 12). The cohesion of this fluid is not strong enough to allow compact dispensing.

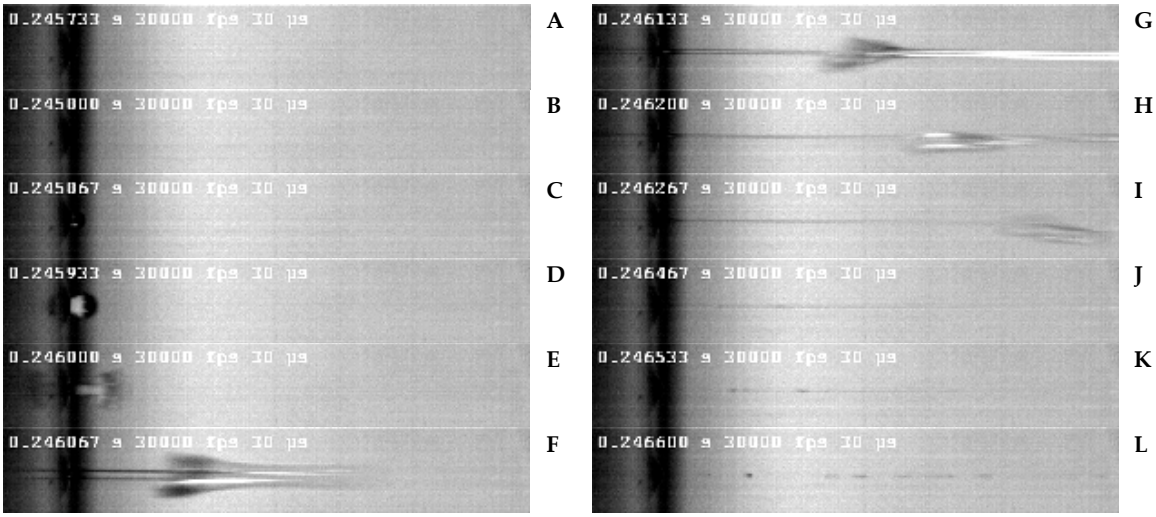

Figure 10. High-speed images of REPDTP drop formation with a time-interval of 67 µs between frames. Left from top to down: Frames 1 to 6. Right from top to down: Frames 7 to 12.

4.2.2. Category II, Underfillers

Similar to the neat resins REPDTP and R0161, the commercial Underfiller R3001 shows a classical start of drop formation in jet phase I, see frames 1 to 6 in Figure 11. As soon as the plunger comes into contact with the nozzle pan, a transition to jet phase II follows. Up to this transition point, the structural evolution with time is comparable to category I materials, except for different damping of the plunger impulse. Considering the Newtonian-like flow behavior and the low viscosity of R3001, its damping ability is impressive since the drop stays compact even after complete impulse transfer into the fluid (frame 7 to 12). During the filament-stretching phase, the evenly formed fluid tail shows a Rayleigh-type breakup [16,21,24] (frame 14).

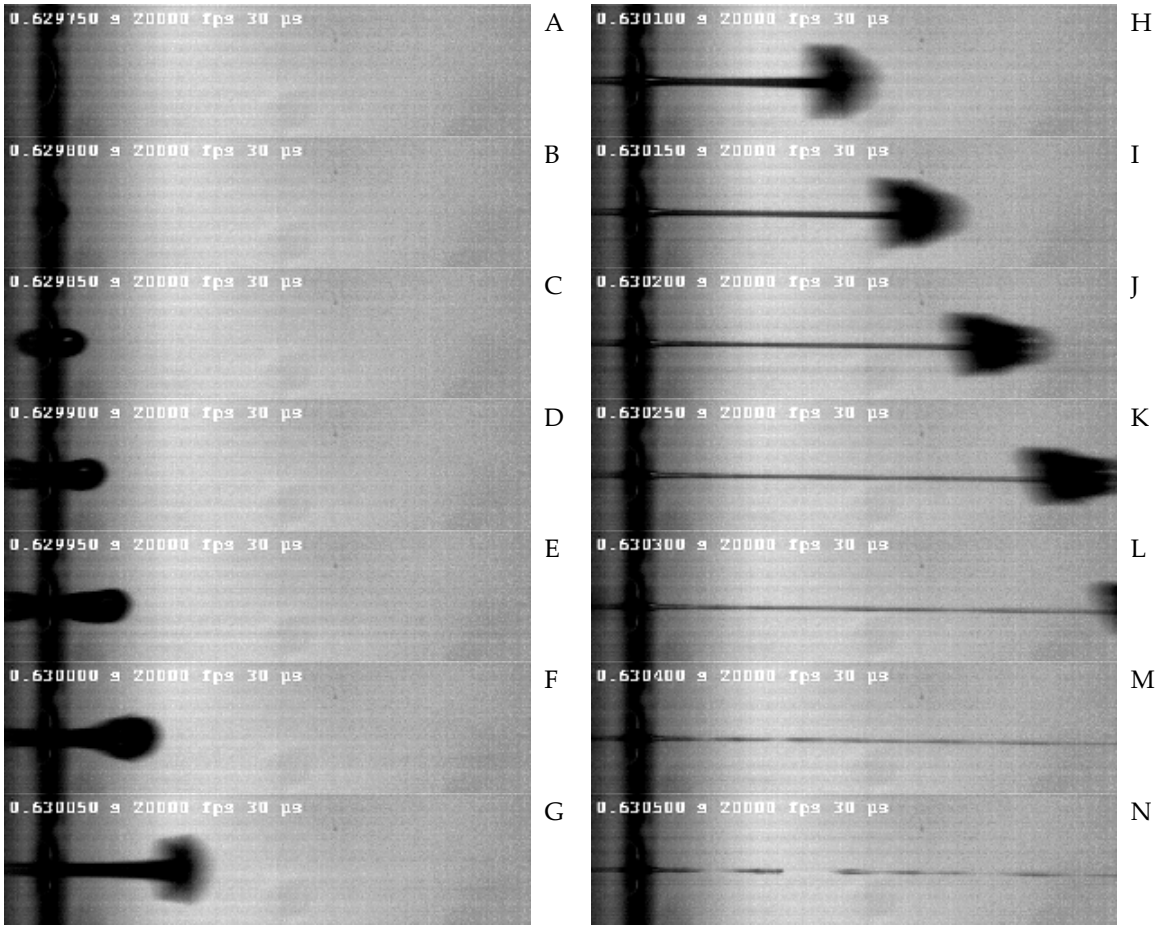

Figure 11. High-speed images of R3001 drop formation with a time-interval of 50 µs between frames. Left from top to down: Frames 1 to 7. Right from top to down: Frames 8 to 14.

4.2.3. Category III, Paste-Like Fluids

Paste-like systems of material category III show a shortened drop dynamic as evidenced by the dispense imagines of REPDTP-R-SiO in Figure 12. Jet phase I is completely overruled and the overall time period is reduced substantially to 0.07 ms in total. As soon as the plunger acceleration reaches a sufficiently large value, the impulse is transferred to the test liquid instantaneously. No damping characteristic can be detected, and a primary thread shoots out of the nozzle orifice. Additionally, no wavelike breakups are observed and the jet stream fractures at a few localized positions into ligands with diameters of approximately 60 µm.

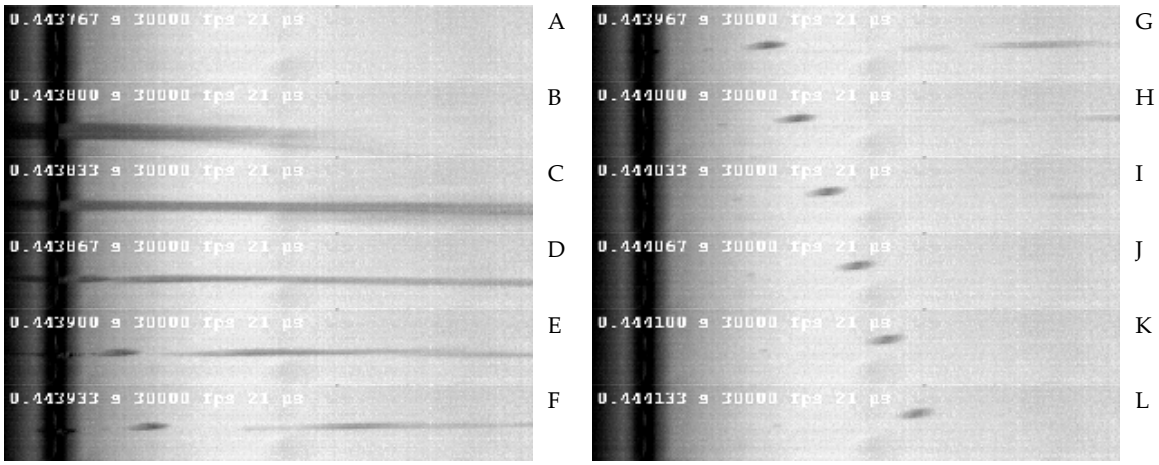

Figure 12. High-speed images of REPDTP-R-SiO drop formation with a time-interval of 33 µs between frames. Left from top to down: Frames 1 to 6. Right from top to down: Frames 7 to 12.

The time-dependent drop deformation stages in terms of positions x_1 and x_2 (beginning and end) of the primary drop/primary thread are presented in Figure 13. For the resins REPDTP and R0161, one can easily observe an abrupt change of slope at 0.35 ms which corresponds to an acceleration of the dispense velocity leading to a steep increase of x_1 and x_2 over time. Different slopes of x_1 and x_2 indicate different velocities of drop tip and drop end and thus a stretching of the thread. Samples REPDTP and REPDTP-R are characterized by a specific starting point for the steep increase of positions x_1 and x_2, as well as a continuous stretching and diameter reduction. We note that for sample REPDTP-R, a delayed transition to jet phase II takes place. During impulse transfer from the plunger to the fluid, the starting point of fluid stretching is shifted to later time frames compared with the unmodified REPDTP. This observation correlates with the rheological data and we conclude that the characteristic jet behavior of REPDTP-R is caused by enhanced viscoelasticity and thixotropy. Thixotropic modifications of REPDTP systematically preserve a low loss modulus G'', as shown in strain sweeps, see Figure 7. Comparing REPDTP-R and R0161-R, both systems have comparable network stability indicated by G', whereas R0161-R does not show a transition from jet phase I to jet phase II after impulse transfer from the plunger to the fluid.

In the case of Underfiller R3001, fluid stretching is delayed relative to impulse initiation as seen from a moderate transition of the slope between 0.2 ms and 0.5 ms in Figure 14. Furthermore, the drop tip and drop end detach from the nozzle with nearly identical velocities. Comparing the drop dynamics with the ones of REPDTP and REPDTP-R, the evenly dispersed glass spheres of R3001 create an additional way to dissipate energy. In contrast to fluids with thixotropic modification and strong network cohesion, particles in Underfillers interact with a non-elastic Newtonian matrix at low flow resistance. Therefore, an impulse injection into the primary drop leads to a viscous deformation. In addition, largely independent glass sphere realignment leads to additional dissipation of impulse energy and compact dispensing of R3001 until a Rayleigh-type breakup occurs.

An equivalent velocity and dispense profile is found for the primary drop of R0161. Once the neat epoxy polymer is modified with Aerosil R805, jet phase I is completely suppressed and only the second phase is observed, see R0161-R in Figure 14. Drop dynamics of REPDTP, R0161, and R3001 are ideal examples of plunger-based jetting and drop evolution as a function of the dispense time. With increasing rheological complexity and high dosage impulses, a strong dispense time decrease occurs for paste-like fluids. The plunger impulse is transferred to the material without any noticeable damping effects. The jetting characteristic of these materials which feature an elastic network in combination with solid particle interactions can be described as solid-like. To overcome the yield stress or the high zero-shear viscosity, all paste-like systems need a high plunger impulse and show identical drop dynamics.

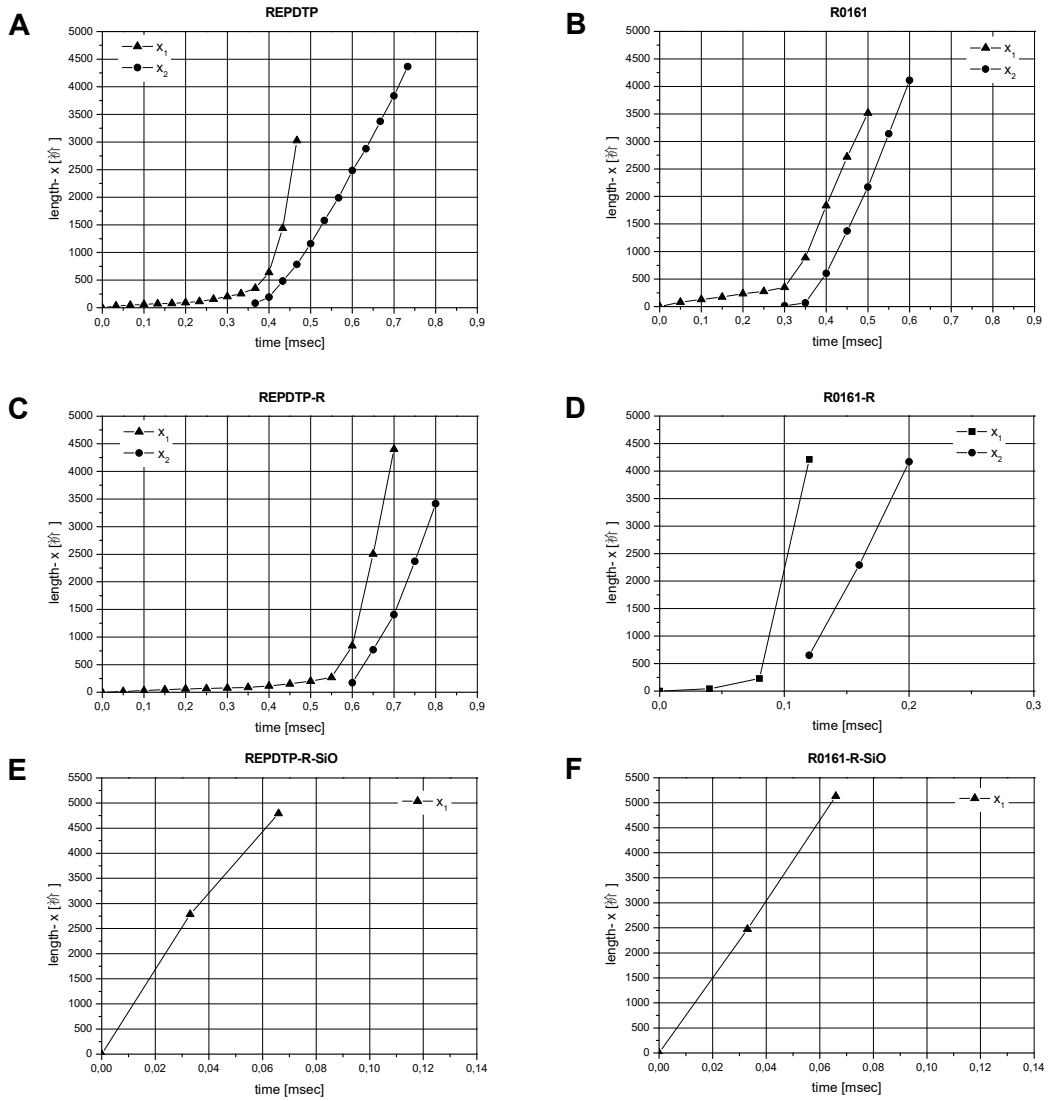

Figure 13. Drop dynamics (positions x1 and x2 of the beginning and end of the primary drop/primary thread) as a function of time for materials of category I (**A**–**D**) and materials of category III in plots (**E**,**F**).

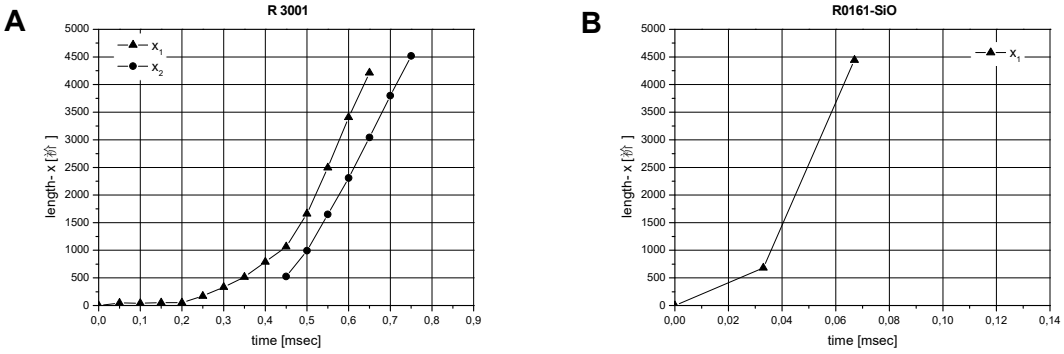

Figure 14. Drop dynamics as a function of time for materials of category II.

5. Discussion and Conclusions

The plunger-based jetting of complex polymer resins can be separated into two stages of material shaping: (a) classical drop formation with a stable structure at low deformation rates and (b) high-speed

deformation with solid-like fluid dispensing. Here we presented a direct correlation between rheology and jet formation.

Test systems with low viscosity and limited structural stability offer a wide spectrum of accessible jet parameters. For systems of material category I, see Table 1, impulse damping and process time up-scaling are documented. The classical drop formation during jet stage I is characterized by various drop contours for identical jet parameters. Based on rheological data, the concept of a damping influence on fluid dispensing was developed. Without microscale particles, the ability of the fluid to reduce the jet impulse is limited, which leads to a continuous primary drop elongation. To verify the concept of a damping influence, the primary drop contour evolution was analyzed as a function of time. Here, a difference in slopes of drop tip and drop end positions reveals a significant damping effect. Changes in the slope of both position curves highlight a change in the relevant damping mechanism and thus a material-dependent influence of rheology.

A peculiarity is found for the commercial system, R3001, which allows for compact dispensing. In this case, only small interactions of the glass spheres with the polymer matrix exist as can be deduced from the sol character and the low viscosity of the fluid. Due to an adjustment of the physicochemical properties of R3001, the internal cohesion nevertheless maintains a compact drop-dispensing characteristic even though an elastic network could not be detected. However, neck thinning of R3001 leads to multiple Rayleigh-type breakups and multiple satellite droplets.

In the case of paste-like fluids, the impact of jet parameters and fluid properties on drop contour evolution becomes negligible. Equivalent drop shapes are obtained for various materials. Despite the fact that in the second jet stage fluid properties are more important than process conditions, a rheological study is generally advised in order to determine the level of dispensability. Glass spheres and thixotropy additives generate an enhanced network stiffness which is characterized by reduced glass sphere mobility within the dispersed Aerosil network. The average deformation range narrows down and shifts to instantaneous material acceleration and primary threads without drop contour. A brittle breakup at the nozzle orifice emerges.

In summary, for a variety of resins and resin modifications, the jetting process was investigated in detail by high-speed imaging. Based on rheological classifications of the materials chosen, the evolution of drop dynamics was studied in different stages of high-speed deformation. In general, the jetting process can be separated into two jet phases and a significant influence on the jet parameters was observed. With the increasing rheological complexity of the materials, jet phase I is suppressed due to dispense impulse reduction by material-specific dampening properties resulting in a stream-like material deposition. Plunger-based jetting was demonstrated to be a versatile technique which allowed for the dosage of all test fluids investigated, regardless of the large variation in the rheological characteristics.

Author Contributions: Conceptualization, A.K. and J.B.; Methodology, A.K.; Validation, J.B. and M.W.; Formal Analysis, A.K.; Investigation, A.K.; Resources, J.B.; Data Curation, A.K. and J.B.; Writing-Original Draft Preparation, A.K.; Writing-Review & Editing, M.W.; Visualization, A.K.; Supervision, J.B. and M.W.; Project Administration, A.K. and J.B.; Funding Acquisition, J.B.

Funding: This research received no external funding.

Acknowledgments: The authors thank VERMES micro dispensing for providing the experimental setup. Furthermore, we thank co-workers from IZM and TU Berlin as well as from the department of Micro Technologies of HTW Berlin for their assistance.

Conflicts of Interest: The authors declare no conflict of interest.

References

1. Rajiv, L.I.; Daryl, L.S. Experimental, Analysis of a Voice-Coil-Driven Jetting System for Micrograms Fluid Depositions in Electronics Assembly. *J. Microelectron. Electron. Packag.* **2017**, *14*, 108–121.

2. Mueller, M.; Franke, J. Feasability study of piezo jet printed silver ink structures for interconnection and condition monitoring of power electronics components. In Proceedings of the 2017 IEEE 19th Electronics Packaging Technology Conference (EPTC), Singapore, 6–9 December 2017; pp. 1–5.
3. Wijshoff, H. Drop dynamics in the inkjet printing process. *Elsevier Curr. Opin. Colloid Interface Sci.* **2018**, *36*, 20–27. [CrossRef]
4. Furbank, R.J.; Morris, J.F. An experimental study of particle effects on drop formation. *Phys. Fluids* **2004**, *16*, 1777–1790. [CrossRef]
5. Dravid, V.; Loke, P.B.; Corvalan, C.M.; Sojka, P.E. Drop Formation in Non-Newtonian Jets at low Reynolds Numbers. *J. Fluids Eng.* **2008**, *130*, 081504. [CrossRef]
6. Richards, J.R.; Beris, A.N.; Lenhoff, A.M. Drop formation in liquid-liquid systems before and after jetting. *Phys. Fluids* **1995**, *7*, 2617–2630. [CrossRef]
7. Soutrenon, M.; Billato, G.; Bircher, F. 3D printing of cellulose by solvent on binder jetting. *Print. Fabr.* **2018**, *4*, 166–169. [CrossRef]
8. Eggers, J. Theory of drop formation. *Phys. Fluids* **1995**, *5*, 941–953. [CrossRef]
9. Badie, R.; De Lange, D.F. Mechanism of drop constriction in a drop-on-demand inkjet system. *Proc. R. Soc. Math. Phys. Eng. Sci.* **1997**, *453*, 2573–2581. [CrossRef]
10. Craster, R.V.; Matar, O.K.; Papageorgiou, D.T. Pinchoff and satellite formation in compound viscous threads. *Phys. Fluids* **2003**, *15*, 3409–3428. [CrossRef]
11. Papageorgiou, D.T. On the breakup of viscous liquid threads. *Phys. Fluids* **1995**, *7*, 1529–1544. [CrossRef]
12. Chen, A.U.; Basaran, O.A. A new method of significantly reducing drop radius without reducing nozzle radius in a drop-on-demand drop production. *Phys. Fluids* **2002**, *14*, L1–L4. [CrossRef]
13. Thoroddsen, S.T.; Etoh, T.G.; Takehara, K. Microjetting from wave focussing on oscillating drops. *Phys. Fluids* **2007**, *19*, 052101. [CrossRef]
14. Meacham, J.M.; Varady, M.J.; Degertekin, F.L.; Fedorov, A.G. Droplet formation and ejection from a micromachined ultrasonic droplet generator: Visualization and scaling. *Phys. Fluids* **2005**, *17*, 100605. [CrossRef]
15. Shin, D.-Y.; Grassia, P.; Derby, B. Numerical and experimental comparisons of mass transport rate in a piezoelectric drop-on-demand inkjet print head. *Int. J. Mech. Sci.* **2004**, *46*, 181–199. [CrossRef]
16. Dong, H.; Carr, W.W.; Morris, J.F. An experimental study of drop-on-demand drop formation. *Phys. Fluids* **2006**, *18*, 072102. [CrossRef]
17. Rothert, A.; Richter, R.; Rehberg, I. Formation of a drop: Viscosity dependence of three flow regimes. *New J. Phys.* **2003**, *5*, 59. [CrossRef]
18. Henderson, D.M.; Pritchard, W.G.; Smolka, L.B. On the pinch-off of a pendant drop of viscous fluid. *Phys. Fluids* **1997**, *11*, 3188–3200. [CrossRef]
19. Xu, Q.; Basaran, O.A. Computational analysis of drop-on-demand drop formation. *Phys. Fluids* **2007**, *19*, 102111. [CrossRef]
20. Taur, A.; Doshi, P.; Yeoh, H.K. Dripping dynamics of Newtonian liquids from a tilted nozzle. *Eur. J. Mech. B/Fluids* **2015**, *51*, 8–15. [CrossRef]
21. Hoath, S.D.; Harlen, O.G.; Hutchings, I.M. Jetting behavior of polymer solutions in drop-on-demand inkjet printing. *J. Rheol.* **2012**, *56*, 1109–1127. [CrossRef]
22. Nazari, A.; Derakhshi, A.Z.; Nazari, A.; Firoozabadi, B. Drop formation from a capillary tube: Comparison of different bulk fluid on Newtonian drops and formation of Newtonian and non-Newtonian drops in air using image processing. *Int. J. Heat Mass Transf.* **2018**, *124*, 912–919. [CrossRef]
23. Winter, H.H.; Chambon, F. Analysis of linear viscoelasticity of a cross-linking polymer at the gel point. *J. Rheol.* **1986**, *32*, 367–382. [CrossRef]
24. Rayleigh, J.W.S. On the instability of a cylinder of viscous liquid under capillary force. *Philos. Mag.* **1892**, *34*, 145–154. [CrossRef]